Topological properties in Hall-magnetohydrodynamics with a strong guide field

L. N. Martin[1], G. De Vita[2], L. Sorriso-Valvo[3,4], P. Dmitruk[1], G. Nigro[2], L. Primavera[2], V. Carbone[2]
[1] *Departamento de Física, Facultad de Ciencias Exactas y Naturales, Universidad de Buenos Aires and IFIBA, CONICET, Buenos Aires 1428, Argentina*
[2] *Dipartimento di Fisica, Università degli Studi della Calabria 87036 Rende (CS), Italy*
[3] *CNR-IPCF - U.O.S. di Cosenza, 87036 Rende (CS), Italy*
[4] *Space Sciences Laboratory, University of California, 94720 Berkeley CA, USA*
(Dated: June 25, 2013)

We present a signed measure analysis of compressible Hall-magnetohydrodynamic turbulence with an external guide field. Signed measure analysis allows to characterize the scaling behavior of the sign-oscillating flow structures and their geometrical properties (fractal dimensions of structures). A reduced numerical model, valid when a strong guide magnetic field is present, is used here. In order to discuss the effect of the Hall term, different values for the ion skin depth are considered in the simulations. Results show that as the Hall term is increased the fractal dimension of the current and vorticity sheets decreases. This observation, together with previous analysis of the same fields, provides a comprehensive description of the effect of the Hall force on the formation of structures. Two main processes are identified, namely the widening and unraveling of the sheets.

I. INTRODUCTION

Magnetohydrodynamics (MHD) is a reasonable theoretical framework to describe the large scale dynamics of a plasma. However, when a more detailed description is needed (for instance, when the physical context favors the development of small scales) it is most appropriate to consider two fluid models. Two fluid effects can be considered through a generalized Ohms law which include the Hall current, which is required for phenomena with characteristic length scales comparable or smaller than the ion skin depth c/ω_{pi} (c is the speed of light, and ω_{pi} is the ion plasma frequency). Among its manifestations, the Hall current causes the magnetic field to freeze in the electron flow instead of being carried along with the bulk velocity field (in an ideal plasma). Another important feature of the ideal Hall-MHD description is the self-consistent presence of electric fields parallel to the mean magnetic field. Hall-MHD has recently been invoked in advancing our understanding of phenomena ranging from dynamo mechanisms [1], magnetic reconnection [2–4], and accretion disks [5, 6] to the physics of turbulent regimes [7–10].

In many cases of interest, such as in fusion devices or geophysical and astrophysical plasmas, a strong externally supported magnetic field is present. In such cases, a new reduced model has been proposed, the RHMHD model [11–13]. In this approximation, the fast compressional Alfvén mode is eliminated, while the shear Alfvén and the slow magnetosonic modes are retained [14]. This new model (RHMHD) is an extension of the previously known reduced MHD (RMHD) model to include the Hall effect. The RMHD equations have been used to investigate a variety of problems such as current sheet formation [15, 16], non-stationary reconnection [17, 18], the dynamics of coronal loops [19–22], and the development of turbulence [23]. The self-consistency of the RMHD approximation has been analyzed in ref. [24]. Moreover, numerical simulations have been used to assess the validity of the RMHD equations by directly comparing its predictions with compressible MHD equations in a turbulent regime [25]. The validity of the RHMHD model has also been studied in the same way [12].

The properties of small scale structures in magnetohydrodynamic (MHD) and Hall-magnetohydrodynamic (HMHD) turbulence have been recently extensively studied. In particular, attention has been paid to the geometrical properties of current sheets in HMHD, as these structures are associated with magnetic flux reconnection and magnetic energy dissipation, processes of uttermost importance in astrophysics and space physics [26–29].

However, studies have provided conflicting results so far, so that the debate on the effect of the Hall term on the generation of turbulent structures is still open. For example, some recent numerical simulations have indicated that current sheets in presence of Hall effect become wider than in MHD (see, e.g., [30]), while, on the contrary, other studies have shown the presence of thinner structures [31].

Previous studies of turbulent HMHD have shown that the peak of the spectrum of the current density is located at wavenumber corresponding to the inverse of the ion skin depth [32–35]. Since this peak can be associated with the average thickness of the current sheets, the shift of the peak was interpreted as a thickening of the current sheets with increasing Hall effect [36]. This result is in good agreement with experimental observations, which confirm that the current sheets thickness in presence of the Hall effect is indeed given by the ion skin depth [37].

On the other hand, other studies have observed formation of thinner structures when Hall effect increases, suggesting that HMHD is more intermittent than MHD [31]. This was also observed in solar wind turbulence, *e.g.* using the Cluster spacecraft magnetic data [38, 39]. Incidentally, other instances of solar wind observations of high-frequency magnetic field fluctuations from the same spacecraft indicated that while large scales are compatible with multifractal intermittent turbulence, small

scales show non-Gaussian self-similarity [40].

Using the set of simulations that will be studied here, in a previous paper the effect of the Hall term has been analyzed in terms of global magnitudes (*e.g.*, the mean square current density $\langle j^2 \rangle$ and vorticity $\langle \omega^2 \rangle$), characteristic times of the flow,energy cascade and qualitative features of the flow structures (current sheets) [30]. The Hall term turned out to affect mostly the scales between the Hall scale and the dissipation scale. This produces an enhancement of the energy transfer in such scale range, and therefore the accumulation of energy decreases. This corresponds to an effective shift of the dissipation scale toward smaller scales. This was estimated by observing an increasingly sharp steepening of the energy spectrum in the Hall range, when the separation between the Hall scale and the dissipation scale is larger. This suggests the possible generation of smaller scales when the Hall effect increases. Qualitative observation of current sheets showed that such smaller scale structures become wider as the Hall effect increases.

In another paper [41], a detailed and rigorous study of intermittency has been performed. In presence of Hall effect, field fluctuations at scales smaller than the ion skin depth become substantially less intermittent, with scaling properties close to self similarity. Numerical simulations quality was also tested, according to the stringent criteria of Wan et al.[42].

The quantitative measure of the intermittency is crucial to understand the topological distribution of dissipation in magneto-fluids and plasmas, and it can also provide constraints for theoretical study of phenomena such as magnetic energy dissipation and reconnection. Following recent results as briefly summarized above, it is thus not clear whether HMHD small scale structures are thinner than in MHD, making HMHD more intermittent than MHD, or, on the contrary, they are more space filling, causing intermittency to decrease because of the Hall effect. The main purpose of the present paper is to quantitatively evaluate the characteristics of the small scale structures and their features with respect to the magnitude of the Hall effect.

In order to gain more insight on the actual effect of the Hall term on flow structures, here we study the geometrical properties of the vorticity and current field, using an explicit and quantitative approach. Our study focuses on the estimation of the cancellation exponents, as introduced by Ott et al. [43]. Such exponents provide a simple characterization of the flows, and are phenomenologically related with the fractal dimension of the typical structure [44]. Finally, corroborated by the aforementioned studies, we show that the Hall effect affects current sheets mainly in two ways. On one hand, the current (and vorticity) sheets widen, while on the other hand they unravel, reaching a more complex topology. This fragmentation, which could be seen as formation of "micro-sheets", turns out to be more and more evident as the Hall effect increases.

The present paper is organized as follows. In Section II, the set of equations describing reduced Hall MHD is described. The details of the numerical simulations are given in Section III. In Section IV the main idea of the cancellation analysis technique is introduced. Finally, results are presented in Section V and discussed in Section VI.

II. REDUCED MHD AND HMHD MODELS

For a compressible flow, the HMHD equations can be written (in dimensionless form) as

$$\frac{\partial \mathbf{u}}{\partial t} - \mathbf{u} \times \boldsymbol{\omega} = -\nabla \left(\frac{\mathbf{u}^2}{2} + \frac{\rho^{\gamma-1}}{M_S^2(\gamma-1)} \right) + \\ + \frac{1}{M_A^2} \frac{\mathbf{J} \times \mathbf{b}}{\rho} + \nu \frac{\nabla^2 \mathbf{u}}{\rho} + \left(\delta + \frac{1}{3}\nu \right) \frac{\nabla(\nabla \cdot \mathbf{u})}{\rho}, \quad (1)$$

$$\frac{\partial \mathbf{A}}{\partial t} - \mathbf{u} \times \mathbf{b} = -\epsilon \frac{\mathbf{J} \times \mathbf{b}}{\rho} - \nabla \phi + \eta \nabla^{\mathbf{2}} \mathbf{A}, \quad (2)$$

$$\frac{\partial \rho}{\partial t} + \nabla \cdot (\rho \mathbf{u}) = 0, \quad (3)$$

$$\nabla \cdot \mathbf{A} = 0. \quad (4)$$

In these equations, $\mathbf{u}$ is the velocity field, $\boldsymbol{\omega}$ is the vorticity field, $\mathbf{J}$ is the current, $\mathbf{b}$ is the magnetic field, ρ is the density of the plasma, and $\mathbf{A}$ and ϕ are respectively the magnetic and electric potentials. A barotropic law is assumed for the plasma, with the pressure given by $p = C\rho^\gamma$, where C is a constant and $\gamma = 5/3$. Equation (4) is the Coulomb gauge, which acts as a constraint that fixes the electric potential in Eq. (2). Control parameters of the system are the sonic Mach number M_S, the Alfvén Mach number M_A, the viscosities ν and δ (here we consider $\nu = \delta$), and the resistivity η. In our study, the most important control parameter is the Hall coefficient $\epsilon = \rho_{ii}/L$, where ρ_{ii} is the ion skin depth and L is the characteristic scale of turbulence. When $\epsilon = 0$, the equations above result in the well known compressible MHD equations.

In the presence of a strong guide field, the equations above can be written using the reduced approximation often used in magnetohydrodynamics (see, e.g., [45, 46]). The approximation assumes that the magnetic field can be written as

$$\mathbf{b} = B_0 \hat{\mathbf{z}} + \mathbf{b}', \quad (5)$$

where B_0 is the intensity of the guide magnetic field aligned with the $\hat{\mathbf{z}}$ direction, and $\mathbf{b}'$ is such that $|\mathbf{b}'|/B_0 \ll 1$.

For convenience, when writing the dimensionless equations we assume, without loss of generality, that $B_0 = 1$.

We then decompose the velocity and magnetic field fluctuations in terms of scalar potentials as

$$\mathbf{u} = \nabla \times (\varphi \hat{\mathbf{z}} + f \hat{\mathbf{x}}) + \nabla \psi, \tag{6}$$

and

$$\mathbf{b}' = \nabla \times (a \hat{\mathbf{z}} + g \hat{\mathbf{x}}) \,. \tag{7}$$

Equation (7) ensures that the magnetic fields remains divergence free, while Eq. (6) gives us a compressible flow. The potentials f and g allow for dynamical components of the fields parallel to the guide field, and ψ describes an irrotational component of the velocity field.

Then, Eqs. (1-4) can be written as (for the details see [47] and [13, 30, 48])

$$\frac{\partial u}{\partial t} = \frac{\partial b}{\partial z} + [\varphi, u] - [a, b] + \nu \nabla^2 u, \tag{8}$$

$$\frac{\partial \omega}{\partial t} = \frac{\partial j}{\partial z} + [j, a] - [\omega, \varphi] + \nu \nabla^2 \omega, \tag{9}$$

$$\frac{\partial a}{\partial t} = \frac{\partial (\varphi - \epsilon b)}{\partial z} + [\varphi, a] - \epsilon [b, a] + \eta \nabla^2 a, \tag{10}$$

$$\frac{\partial b}{\partial t} = \beta_p \frac{\partial (u - \epsilon j)}{\partial z} + [\varphi, b] + \beta_p [u, a] + \\ - \epsilon \beta_p [j, a] + \eta \beta_p \nabla^2 b, \tag{11}$$

where

$$u = -\partial_y f, \tag{12}$$
$$\omega = -\nabla_\perp^2 \varphi, \tag{13}$$
$$b = -\partial_y g, \tag{14}$$
$$j = -\nabla_\perp^2 a, \tag{15}$$

and the notation $[A, B] = \partial_x A \partial_y B - \partial_x B \partial_y A$ is employed for the Poisson bracket. The potential ψ was eliminated from these equations using the equation for the pressure. Finally, $\beta_p = \beta\gamma/(1 + \beta\gamma)$ is a function of the plasma "beta". As in the previous set of equations, these equations become the compressible RMHD equations when $\epsilon = 0$.

III. NUMERICAL SIMULATIONS

Simulations analyzed in this work are similar to those described in Ref. [30]. We use a standard parallel pseudo-spectral code to evaluate the nonlinear terms and solve numerically the equations [49]. A second-order Runge-Kutta time integration scheme is used. The magnetic field fluctuations in all simulations are less than ten percent of the external magnetic field value, so we are in the range of validity of the RHMHD model. Periodic boundary conditions are assumed in all directions of a cube of side $2\pi L$ (where $L \sim 1$ is the initial correlation length of the fluctuations, defined as the length unit). The runs performed throughout this paper do not contain any magnetic or velocity external stirring terms, so the RHMHD system is let to evolve freely. To generate the initial conditions, we excite initially Fourier modes (for both magnetic and velocity field fluctuations) in a shell in k-space with wave numbers $1 \leq k \leq 2$, with the same amplitude for all modes and with random phases. Only plane-polarized fluctuations (transverse to the mean magnetic field) are excited, so the initial conditions are Alfvén mode fluctuations with no magnetosonic modes. In the set of simulations, spatial resolution is 512^2 grid points in the plane perpendicular to the external magnetic field and 32 grid points in the parallel direction. In fact, higher resolution is required in the planes perpendicular to B_0, with respect to the parallel direction. This is due to the fact that the dynamics of the system generates structures mostly along the direction perpendicular to B_0. The kinetic and magnetic Reynolds numbers are defined respectively as $R = 1/\nu$, $R_m = 1/\eta$, based on unit initial r.m.s. velocity fluctuation, unit length, and dimensionless values for the viscosity and diffusivity. For all the runs, we used $R = R_m = 1600$ (i.e., $\nu = 1/1600$, $\eta = 1/1600$). We also considered a Mach number $M_S = 1/4$, and an Alfvén Mach number $M_A = 1$.

Four values of the Hall parameter were considered, namely $\varepsilon = 0$ (MHD case), 1/32, 1/16, and 1/8. Data from simulations with such values of ε will be labeled as Run 1, 2, 3 and 4, respectively. As the numerical domain used has size 2π (see above), these values correspond respectively to ion skin depths with associated wave numbers $k_\varepsilon = \infty$, 32, 16, and 8, and to scales of ρ_{ii} =0, 0.03, 0.06 and 0.4.

[LUIS, IF YOU WANT TO PUT THE TABLE, PLEASE DO IT HERE, OTHERWISE PLEASE REMOVE ALL REFERENCES TO THE TABLE (THERE SHOULD BE 2)] Figures 1 and 2 show some example of current components. Left hand panels show, for each Run, two dimensional cuts in the perpendicular plane of one perpendicular component j_x (Figure 1) and of the parallel component j_z (Figure 2), for one snapshot of the simulation in the statistically steady state (when $t = 4.5$). On the right panels, the same field is plotted with an arbitrary tilt angle, in order to highlight the chaotic alternation of positive and negative fluctuations of the fields. From visual inspection, it appears evident that structures become more fragmented as ε increases. Figure 3 shows the total energy spectra $E(k)$, integrated on spheres of radius k, for the four runs. The ion skin depth scale is also indicated. The large scale part of the spectra is compatible with the typical Kolmogorov scaling $\alpha = 5/3$. For the largest ε (Run 4), a secondary power-law region emerges at scales smaller than the ion skin depth, compatible with the typical spectral index for reduced Hall MHD, $\alpha = 7/3$.

It was recently stressed that well resolved numerical

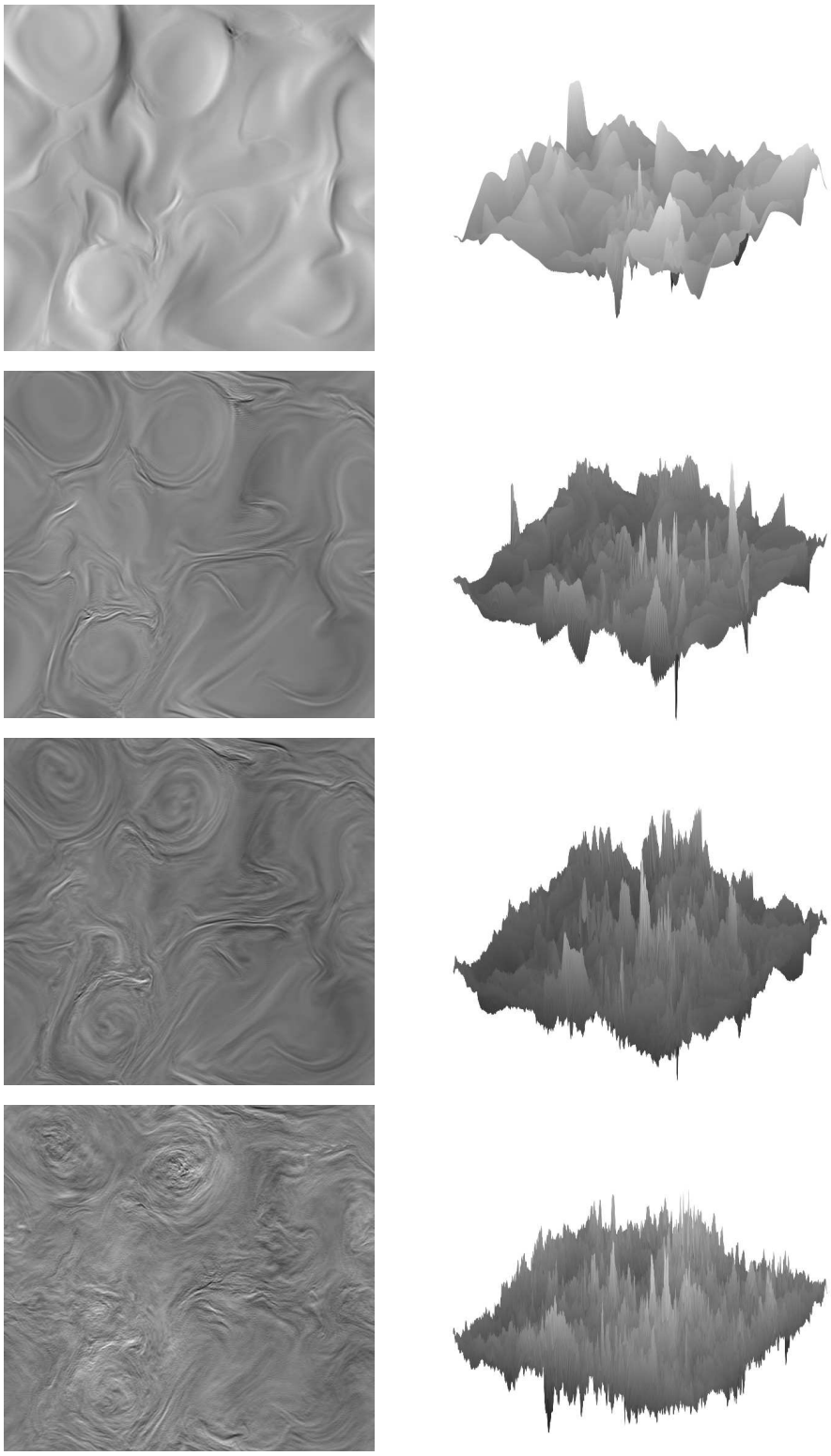

FIG. 1: Left panels: slices of the perpendicular current component j_x in the perpendicular plane, for the snapshots and the four different values of ε used in this work (ε increasing from top to bottom). Right panels: the same fields, seen at an arbitrary tilt angle, highlighting the presence of alternate sign structures at all scales. The scale of grays is arbitrary.

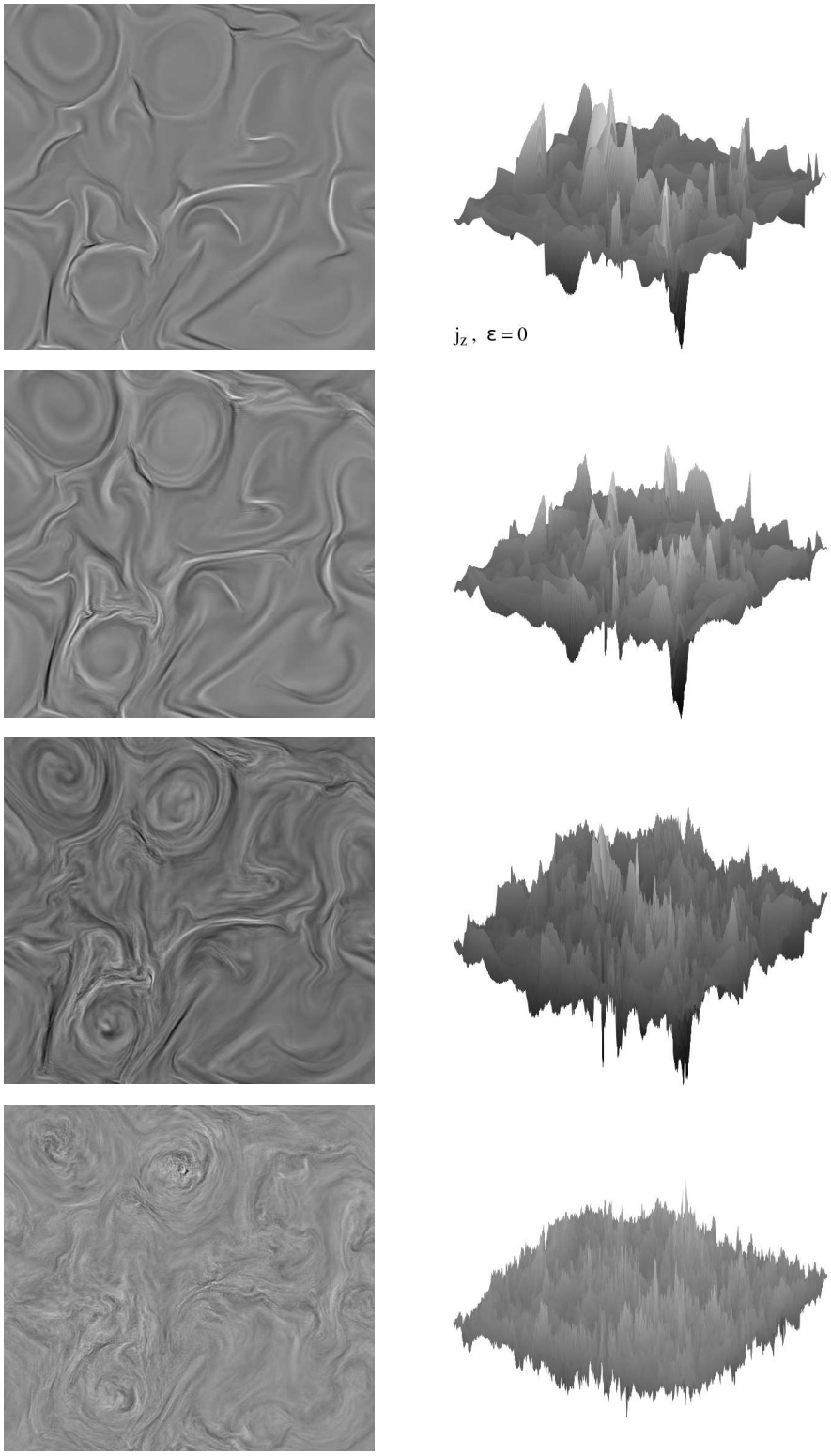

FIG. 2: Left panels: slices of the parallel current component j_z in the perpendicular plane, as in previous figure. Right panels: the same fields, seen at an arbitrary tilt angle.

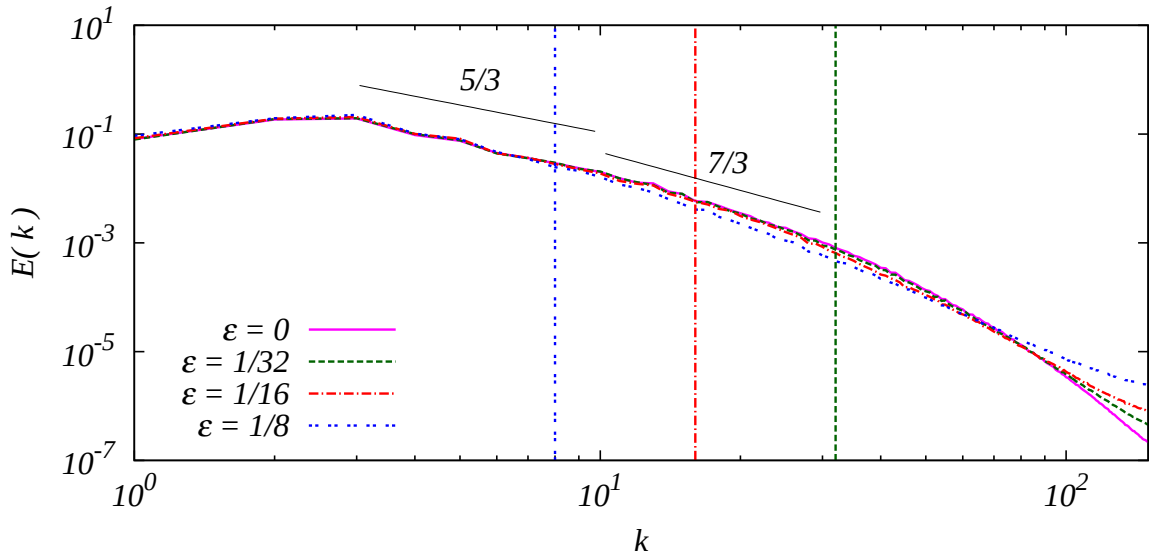

FIG. 3: The total energy spectra for the four Runs (see legend). Phenomenological predictions for the MHD range and for the Hall range are also indicated

simulations are necessary in order to accurately quantify high order statistics and intermittency in MHD [42]. In particular, it has been claimed that if the flow is not properly resolved, a partial thermalization of the small scales may result in artificial Gaussian statistics and an artificial decrease of the intermittency. Wan et al. [42] also argued that an MHD simulation can be considered well resolved, if the kurtosis of the current is independent on the spatial resolution. In order to evaluate the sensitivity to the grid resolution of our system, two different realizations have been performed with higher spatial resolution of $768^2 \times 32$ and $512^2 \times 64$ grid points, respectively. Using the same set of parameters, diagnostics such as structure functions, scaling exponents, and PDFs of field fluctuations have been used to show that scaling and intermittency properties are not affected by resolution. In the MHD and HMHD runs analysed here, the requirement of kurtosis convergence is fulfilled, at least up to the level of expected statistical fluctuations. It is thus possible to conclude that the simulations are well resolved, and satisfies the stringent criteria of Wan et al. [42]. The resolution analysis is shown in detail in the Ref. [41].

IV. THE SIGNED MEASURE AND THE CANCELLATION EXPONENT

As discussed in the introduction, turbulent plasmas are often characterized by scale dependent formation of energetic and localized structures. These represents regions where dissipation of energy is enhanced, and are believed to be responsible for the anomalous scaling of the structure functions. Intermittency and multifractality are strictly related to their presence [50]. Structures such as current sheets and vorticity filaments are continuously observed in numerical simulations [31, 51–55]. Solar wind measurements have also revealed the presence of structures of different type (current sheets, rotational discontinuities, vortices) [56–59]. Since structures can be seen as smooth regions embedded in a highly fluctuating field, they can be associated to scale dependent changes of the sign of the fields gradients. The introduction of a sign-singular measure (as opposed to a positive defined probability measure) allows the characterization of the scaling properties of sign oscillations of the fields [43]. The signed measure of a mean-less scalar field $f(\mathbf{r})$, defined on a d-dimensional set $Q(L)$ of size L, can be introduced as follow. Let $\{Q_i(l)\} \subset Q(L)$ be a partition of $Q(L)$ in disjoint subsets of size l. Then, for each scale l and for each set of boxes $Q_i(l)$, the signed measure is defined as

$$\mu_i(l) = \frac{\int_{Q_i(l)} \mathrm{d}\mathbf{r}\ \mathbf{f}(\mathbf{r})}{\int_{Q(L)} \mathrm{d}\mathbf{r}\ |\mathbf{f}(\mathbf{r})|}\ . \tag{16}$$

As the scale of the subset $Q_i(l)$ increases, cancellations between small size structures of opposite sign become more probable within each box. The way this happens can be statistically characterized through the partition function

$$\chi(l) = \sum_{Q_i(l)} |\mu_i(l)| \tag{17}$$

where the sum is extended to all disjoint subset $Q_i(l)$. When the partition function shows power law scaling $\chi(l) \sim l^{-\kappa}$, the measure is said *sign singular*, and κ is called *cancellation exponent*, representing a quantitative measure of the cancellation efficiency. For

example, a smooth field has constant partition function ($\kappa = 0$), whereas for a stochastic process $\kappa = d/2$ ([60]). More generally, if a field $\mathbf{g}(\mathbf{r})$ is homogeneous with a Hölder scaling exponent h, that is if $\langle \|\Delta\mathbf{g}(\mathbf{l})\| \rangle = \langle \|\mathbf{g}(\mathbf{r}+\mathbf{l}) - \mathbf{g}(\mathbf{r})\| \rangle \sim l^h$, then the cancellation exponent of its derivative $f \equiv \mathrm{d}g/\mathrm{d}r$ is $\kappa = 1 - h$ [60, 61]. Thus, cancellation exponents characterize the topology of structures. A simple geometrical argument, based on the separation of the field in correlated (the structures) and uncorrelated (the background field) subsets, allows to establish a phenomenological relationship between the cancellation exponent and the fractal dimension D of the typical dissipative structures of the flow

$$\kappa = (d - D)/2 \tag{18}$$

(see e.g. [44] for details). It should be kept in mind that, because multifractality is ubiquitous in MHD turbulence, the use of one single fractal dimension cannot capture all the features of the scaling. Nonetheless, D still represents a useful indicator for the topological characteristics of the "mean" intermittent structures of the flow. Cancellation analysis has been performed in the past to describe the formation of structures in two dimensional MHD plasmas [44, 62], and successfully applied to solar active regions, where the time evolution of the topological properties of the surface current has allowed to predict the occurrence of large flares [63–65].

In this paper, we show results of the cancellation analysis of the fields with the aim of pointing out the effect of the Hall term on the topology of the small scales structures.

V. RESULTS

For our analysis, we have considered four snapshots of RHMHD simulations, realized using four different values of the Hall parameter ε, as indicated in Section III. All the snapshots are taken in a statistically steady state of the system, realized when $t = 4.5$. The fields anlyzed here are the three components of the current $\mathbf{j}$ and of the vorticity ω, already shown in Figures 1 and 2. To estimate the partition functions, we divided the simulation domain of size $L^3 = (2\pi)^3$ in boxes of variable size $l_x \times l_y \times l_z$, with $l_x = l_y = l_\perp$ and $l_z = l_\parallel$.

Figure 4 shows some examples of two dimensional cuts of the signed measure computed for the parallel component of the current j_z in the plane x-y, for two values of ε, and for four different partition box sizes. It is evident that the coarse graining of the set partition leads to cancellations at larger scales, so that small scale structures (the current filaments clearly evident at small scale, see left panel) gradually disappear. Similar behavior is seen for all fields components, and for any value of the Hall parameter (not shown).

From the signed measures, partition functions (17) have been computed for all components of the current $\mathbf{j}$ and of the vorticity ω as a function of the two scale parameters $l_\perp$ and $l_\parallel$. Examples of the results are presented in Figure 5. While it is evident that scaling properties are present and well developed in the perpendicular direction $l_\perp$, the partition functions decrease with the parallel scale $l_\parallel$ is somewhat smoother and less defined. This is due to the fact that in RHMHD the turbulent cascade is mainly developed in the perpendicular planes. For this reason, we will mainly concentrate on the scaling properties in the perpendicular planes, by selecting one particular parallel scale. We analyzed the results for different parallel scales, and no significant difference was observed.

Figures 6 and 7 show examples of the partition functions of the fields for a fixed value of $l_\parallel = 0.03$, and for different ε. When appropriate, power law fits $\chi(l_\perp) \sim l_\perp^{-\kappa}$ have been performed through a least square method. The fitting curves are diplayed in the figures. For a visual test, the partition functions have been compensated by dividing them by the fitted power law $l_\perp^{-\kappa}$, and represented in the bottom panels of each figure. Scaling ranges are seen as flat regions in the compensated plots. Compensated plots and fitting power laws have been represented as full lines for the Hall range, and with double-dahsed lines for the MHD range.

As can be seen in all panels of figures 6 and 7, the partition functions suggests presence of power law scaling, and therefore sign singularity, in a range of perpendicular scales corresponding to the inertial range of the energy spectra (cf. figure 3). This holds for all fields and Hall parameters, and is the signature of the MHD turbulent cascade among structures of different size [44]. A second power law range emerges at small scales when the strength of the Hall term increases (panels g-h of figures 6 and 7). This suggests that a secondary sign singularity is present, with fragmentation of dissipative structures along the scales, presumably due to the nonlinear Hall cascade. The small scale power law is observed for the current and vorticity components lying on the plane perpendicular to B_0, while for the parallel components the secondary sign singularity only appears for the largest value of ε analyzed here (panels g and h). This is in agreement with the emergence of a small scale power law range in the energy spectra (see figure 3), which has HMHD phenomenological spectral index.

As mentioned in previous Section, values of the cancellation exponents provide information on the topology of the fields. In order to discuss more easily the analysis results, cancellation exponents have been converted into the typical fractal dimension of the structures, as $D = 3 - 2\kappa$. Values of D are then displayed in Figure 8 as a function of ε, for the three components of the current (panels a and c) and of the vorticity (panels b and b), so that the influence of increasing Hall effect on the scaling can be evaluated. In the following, we will use the notation $D_\perp^{(f)}$ for fractal dimension estimated for the perpendicular partition function $\chi(l_\perp)$, and $D_\parallel^{(f)}$ for the parallel partition function $\chi(l_\parallel)$, where $f = j, \omega$ indicates

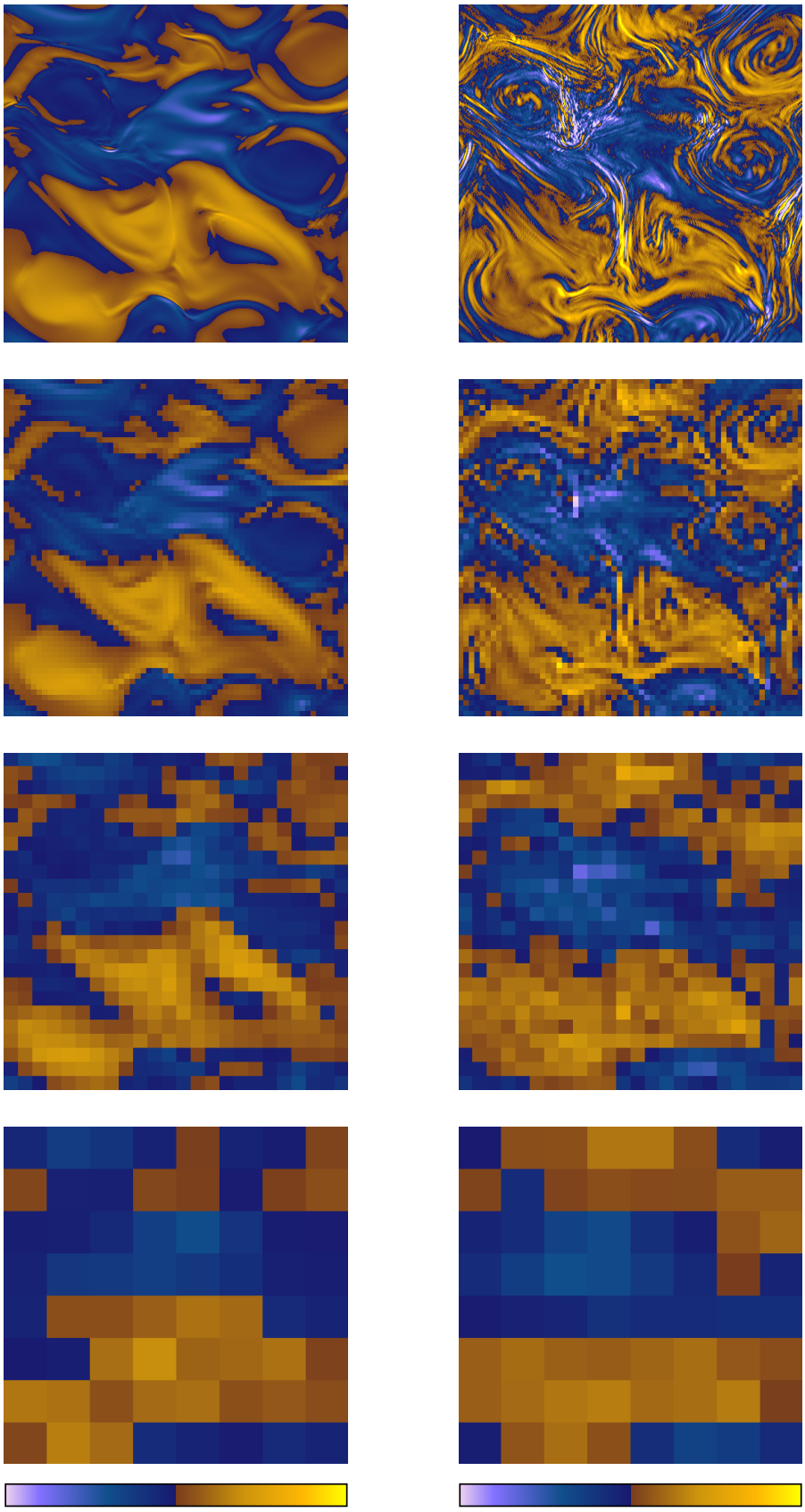

FIG. 4: The signed measure μ as estimated for j_x in the plane y-z, for Run 1 ($\varepsilon = 0$, left panels) and Run 3 ($\varepsilon = 1/16$, right panels), for four different partition box sizes (from top to bottom, $l_\perp = 0.12$, 0.04, 0.016 and 0.002). The color scale is arbitrary.

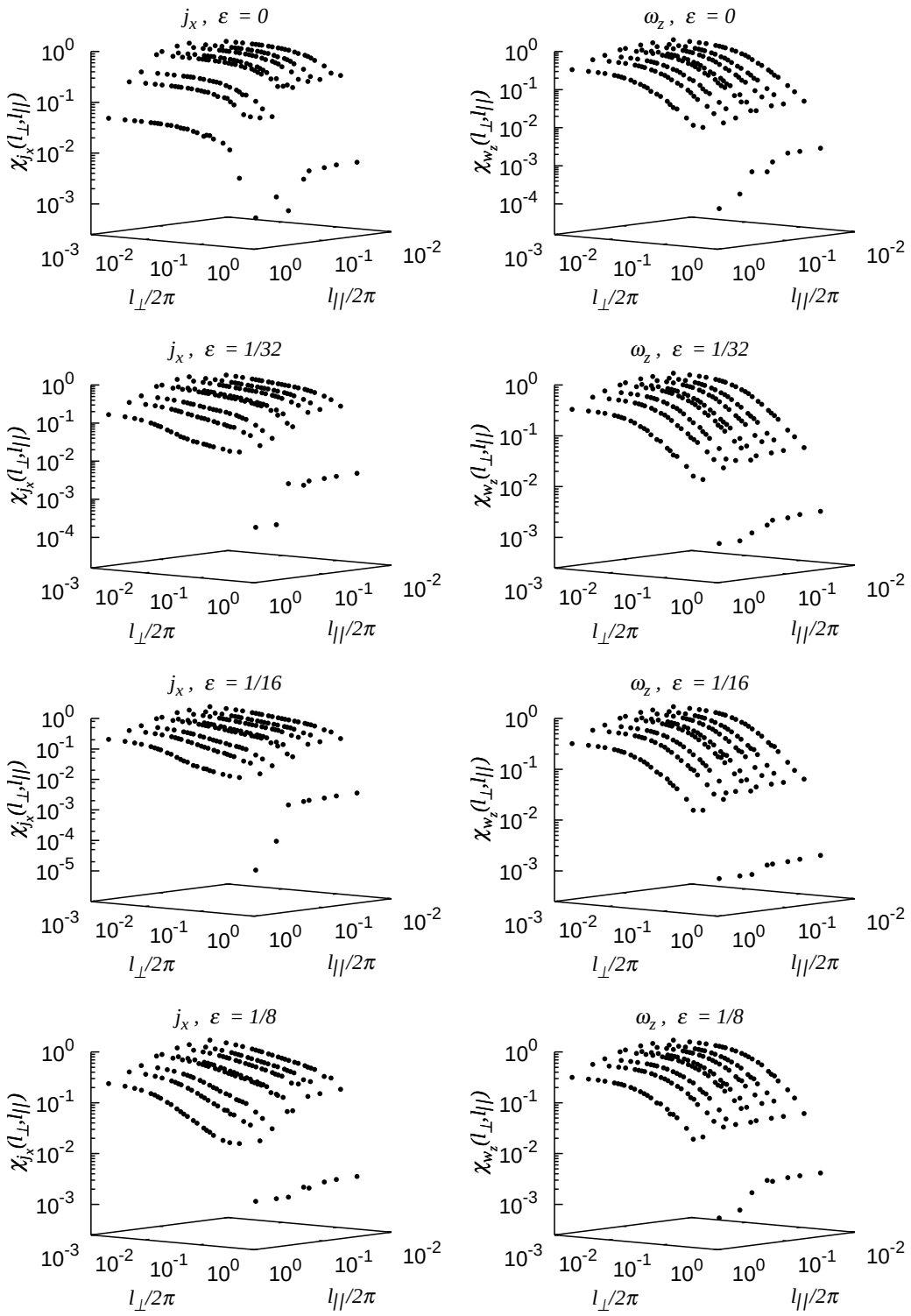

FIG. 5: The partition function $\chi(l_\perp, l_\parallel)$ versus the two scale parameters $l_\parallel$ and $l_\perp$. The examples given here refer to the parallel components of the current (j_z, left hand plots) and one of the perpendicular components of the vorticity (w_x, right hand plots), for the four values of the Hall parameter (sorted from top to bottom for increasing ε, as indicated in each plot).

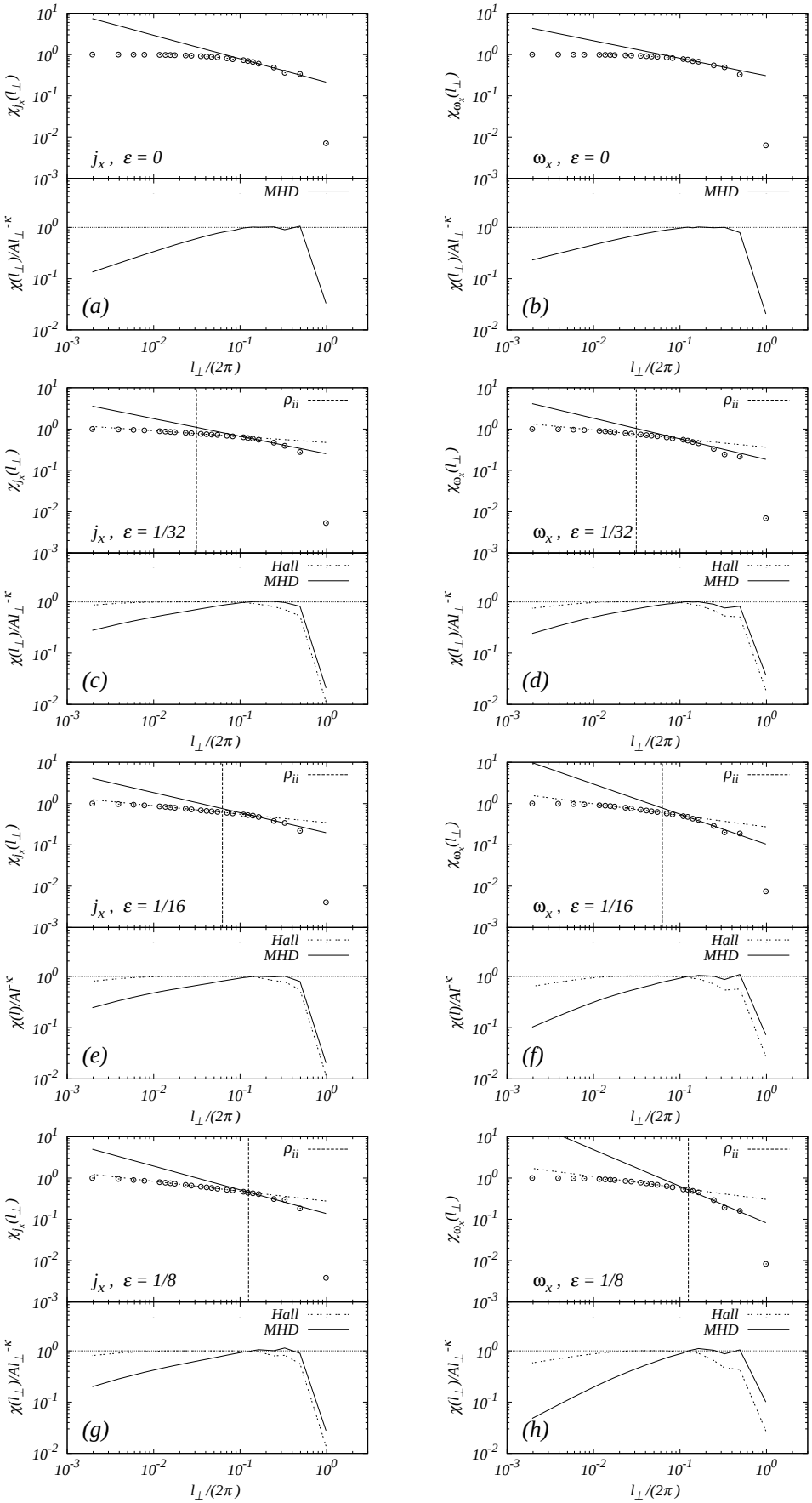

FIG. 6: The partition function $\chi(l_\perp)$ versus the scale parameter $l_\perp$ for j_x (left) and ω_x (right), for the four runs (ε increasing from top to bottom), and at $l_\parallel/2\pi = 0.03$. Power law fits $\chi(l_\perp) = A(l_\perp/2\pi)^{-\kappa}$ are superimposed. The ion skin depth is indicated (dashed line). Finally, the bottom part of each plot shows the compensated partition function $\chi(l_\perp)/A(l_\perp/2\pi)^{-\kappa}$.

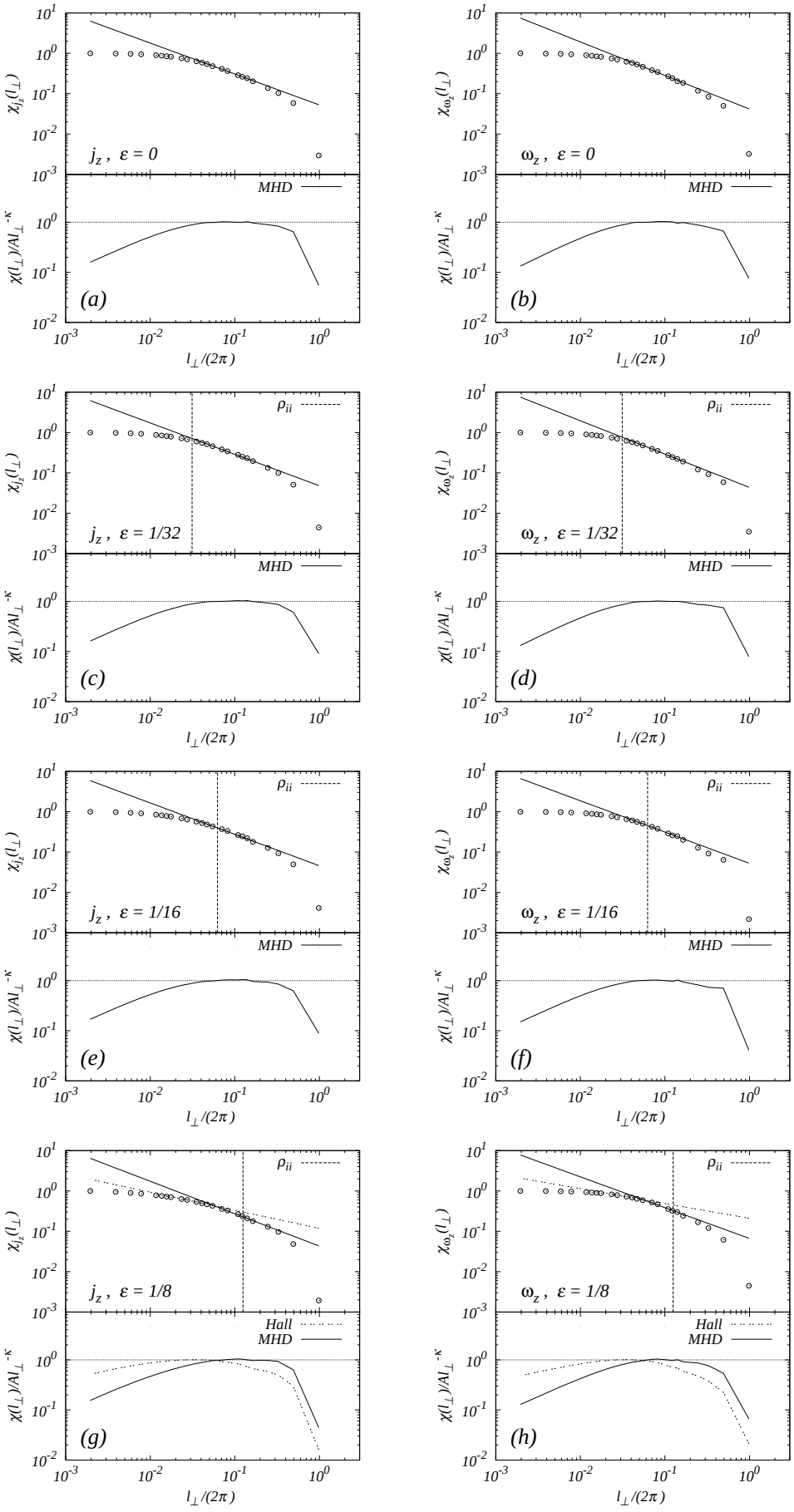

FIG. 7: Same as Figure 6, for the parallel component: j_z (left hand plots) and ω_z (right hand plots).

the field under study. When the superscript $^{(f)}$ is omitted, we are indicating both fields. It is also possible to introduce a parameter for estimating the "global" fractal dimension of the fields, by averaging the three values $D_i^{(f)}$ of the fractal dimension obtained for the i-th component of each field f, $D_\perp^{\star(f)} = (D_x^{(f)} + D_y^{(f)} + D_z^{(f)})/3$ (we have temporarily suppressed the subscript $\perp$ in this formula, to semplify the notation).

We remind the reader that, in the RHMHD configuration, most of the nonlinear structures are generated in the plane perpendicular to B_0. Therefore, the parallel component of the current j_z and vorticity ω_z, which depend on the perpendicular components of the magnetic and velocity fields, are of particular interest. The perpendicular components j_x, j_y, ω_x, ω_y, on the contrary, include both the perpendicular and parallel components of magnetic and velocity fields. This results in mixing the turbulent perpendicular dynamics with the quasi-linear parallel dynamics, so that results are not easily interpreted.

In the MHD inertial range, marked as "MHD" in the figures, the estimated fractal dimension for the parallel component of the current is almost constant, showing a weak decrease from $D_\perp^{(j)} = 1.5$ in the MHD regime to $D_\perp^{(j)} = 1.4$ in the Hall regime (red plot in Figure 8, panel *a*). Similar values, but with opposite weak trend, are observed for the vorticity ω_z (panel *b*). Such values of D are representative of severely disrupted, almost filamented current sheets. The relative independence of $D_\perp^{(j)}$ on the Hall parameter for the parallel components of vorticity and current is consistent with the fact that, in the MHD inertial range, the Hall term is not expected to play a relevant role, since it should only be effective at smaller scales.

For the current perpendicular components (green and blue plots in Figure 8, panel *a*), $D_\perp^{(j)}$ starts around 2 (indicating current sheets) with no Hall effect. As the Hall term is turned on, the dimension first weakly increases to about $D_\perp^{(j)} \simeq 2.2$, and then steadily decreases back to $D_\perp^{(j)} \simeq 2$, showing that structures are becoming more complex. This suggests that inertial range fields are reacting to the onset of the Hall effect, probably in response to the inertial range modification. For the vorticity components perpendicular to B_0 (green and blue plots in Figure 8, panel *b*), the effect of the Hall term is even more evident, causing a decrease of the dimesion from $D_\perp^{(\omega)} \simeq 2.3$ to $D_\perp^{(\omega)} \simeq 1.5$, indicating with fragmentation of the vorticity sheets. The "global" fractal dimensions $D_\perp^\star$ are shown in Figure 8, panel *e* (for the current) and panel *f* (for the vorticity), for both the MHD and Hall ranges. For the current in the MHD range, the structures topology is roughly constant for all values of the Hall effect. Vorticity, on the contrary, shows a more evident decrease of the "global" fractal dimension with ε, from $D_\perp^{\star(\omega)} \simeq 2.3$ to $D_\perp^{\star(\omega)} \simeq 1.5$. This result shows that magnetic field and velocity are decoupled in the MHD range, so that the their structures have different topological properties.

We now turn our attention to the range of scales smaller than the ion skin depth, where the Hall term becomes relevant when ε becomes larger. Results here are very similar for both current and vorticity, suggesting that velocity and magnetic fields decouple only in the MHD range. If no Hall cascade is present ($\varepsilon = 0$, see panels *a* and *b* of figures 6 and 7), the small scale range is characterized by smooth fluctuations (for which we assume $D_\perp = 3$) for all components of the fields, as expected when dissipation is active and numerically well resolved. This is reflected in the absence of power law, or sign singularity, in the transition from the MHD range toward the constant partition function value for smooth fields ($\chi = 1 \rightarrow \kappa = 0 \rightarrow D = 3$) at small scales. As the Hall effect comes into play, the perpendicular components of current and vorticity start to develop a power law range, with cancellation exponents κ increasing with ε (panels *c*-*f* of figure 6). The scaling of the partition function indicates the presence of strongly persistent structures, in the range of scales larger than the typical dissipative scales. In terms of fractal dimension (green and blue plots in Figure 8, panels *c* and *d*), a decrease is observed from $D_\perp = 3$ to $D_\perp \simeq 2.4$, indicating that the smooth fields in the MHD regime (Run 1) are developing toward more complex, broken structures (Runs 2, 3 and 4). On the other hand, for the parallel component of current and vorticity the sign singularity in the Hall range is only observed at $\varepsilon = 1/8$ (see panels *c*-*f* of figure 7). At this value of the Hall parameter, the field is no longer smooth (as instead happens for dissipative range), but rather shows presence of quasi two-dimensional sign persistent structures (red plots in Figure 8, panels *c* and *d*). At these small scales, the "global" fractal dimension calculated for the current and the vorticity steadily decreases from $D_\perp^\star = 3$ to $D_\perp^\star \simeq 2.3$ as the Hall term coefficient increases, confirming once more that the turbulent stuctures are being fragmented by the nonlinear Hall cascade.

Finally, we quickly review the results obtained for the scaling in the parallel direction. Figure 9 shows some examples of partition functions of the current and vorticity components, as a function of the parallel scale, $\chi(l_\parallel)$. partition functions were estimated for $l_\perp/2\pi = 0.002$. As evident, the power law range is severely reduced because of the lower resolution of the numerical simulations. However, we have fitted the partition functions with the usual power law, obtaining the cancellation exponents κ and, therefore, the fractal dimensions D. These are shown in figure 10 as a function of the Hall parameter. As expected from the RHMHD model, for both fields the component parallel to the magnetic field has almost constant $D_\parallel \simeq 2.2$ (see the red plots in panels *a* and *b* of figure 10). On the contrary, for the two components on the perpendicular plane, $D_\parallel$ increases with ε from very small values ($D_\parallel \simeq 0.8$) to about $D_\parallel \simeq 1.9$ (green and blue plots in panels *a* and *b* of figure 10), similarly to what is

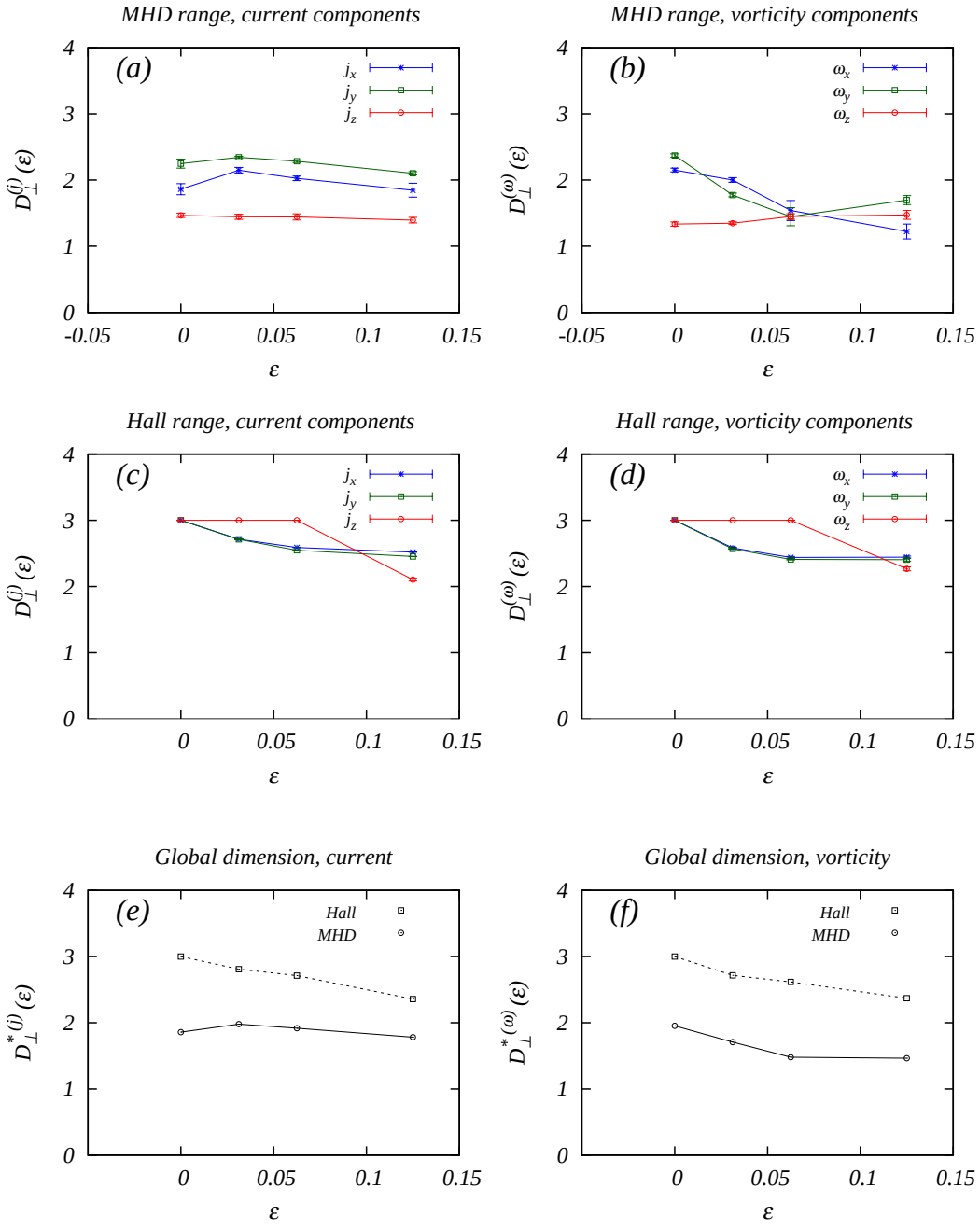

FIG. 8: The fractal dimension $D_\perp$ estimated through equation 18, for the three components of current (a for the MHD range, c for the Hall range) and vorticity (b for the MHD range, d for the Hall range), labeled with different colors and line style (see inset). The indicators $D_\perp^\star$ (see text) are also plotted for the two fields (panels e and f, black lines).

observed for the perpendicular partition functions. The "global" fractal dimension increases from $D_\parallel^\star = 1.3$ to $D_\parallel^\star = 2$.

VI. CONCLUSIONS

In this paper, a set of simulations of a RHMHD flow realized with different values of the Hall parameter ϵ, was analyzed by using the sing-singular measure. The presence of power law scaling of the partition function was observed in two distinct ranges of scales, corresponding to the MHD and Hall MHD ranges. This is interpreted

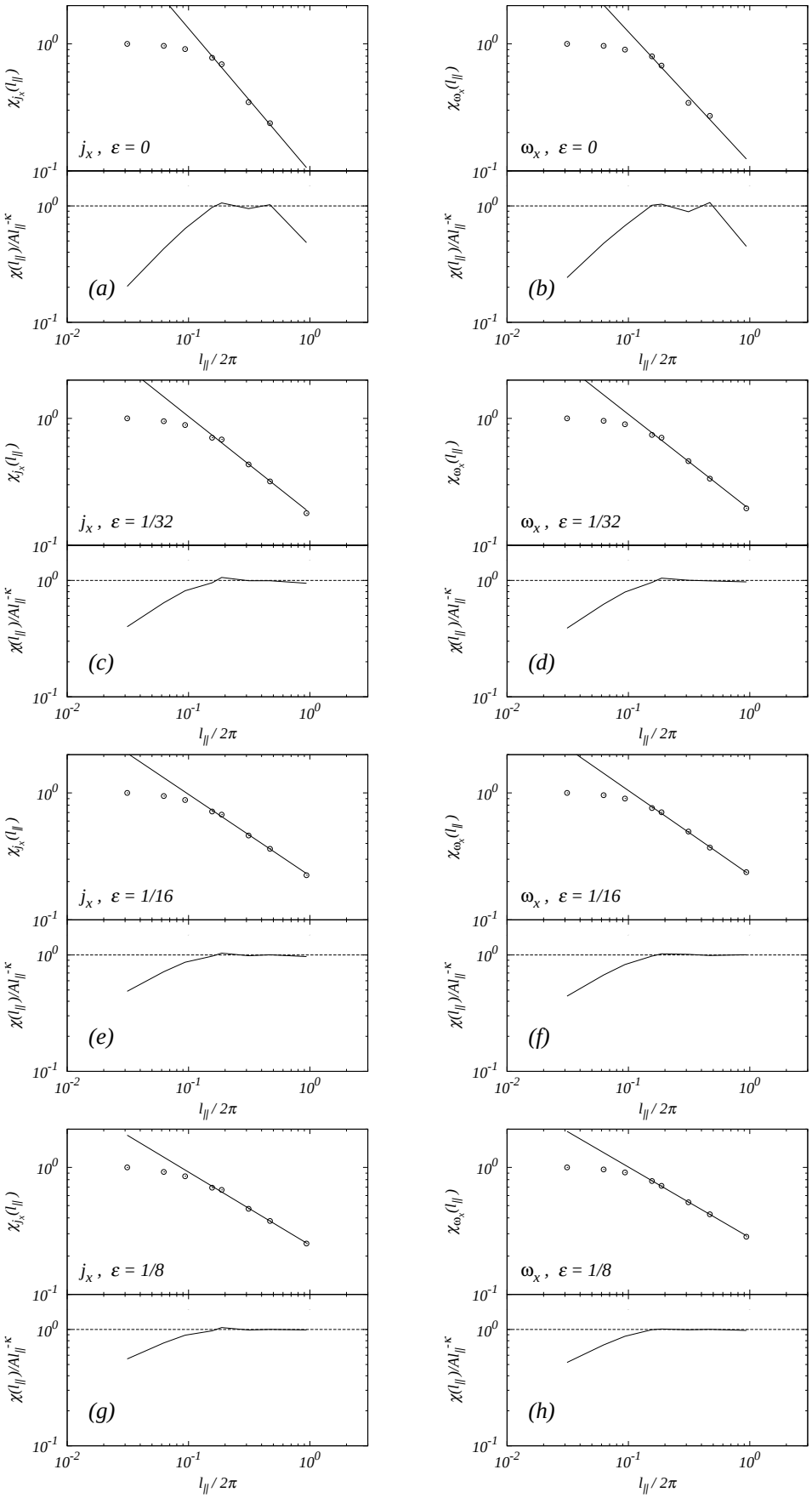

FIG. 9: The partition function $\chi(l_\parallel)$, for j_x (left) and ω_x (right), for the four runs (ε is indicated in each plot), and at $l_\perp/2\pi = 0.002$. Power law fits are superimposed. The bottom part of each plot shows the compensated partition function $\chi(l_\parallel)/A(l_\parallel/2\pi)^{-\kappa}$.

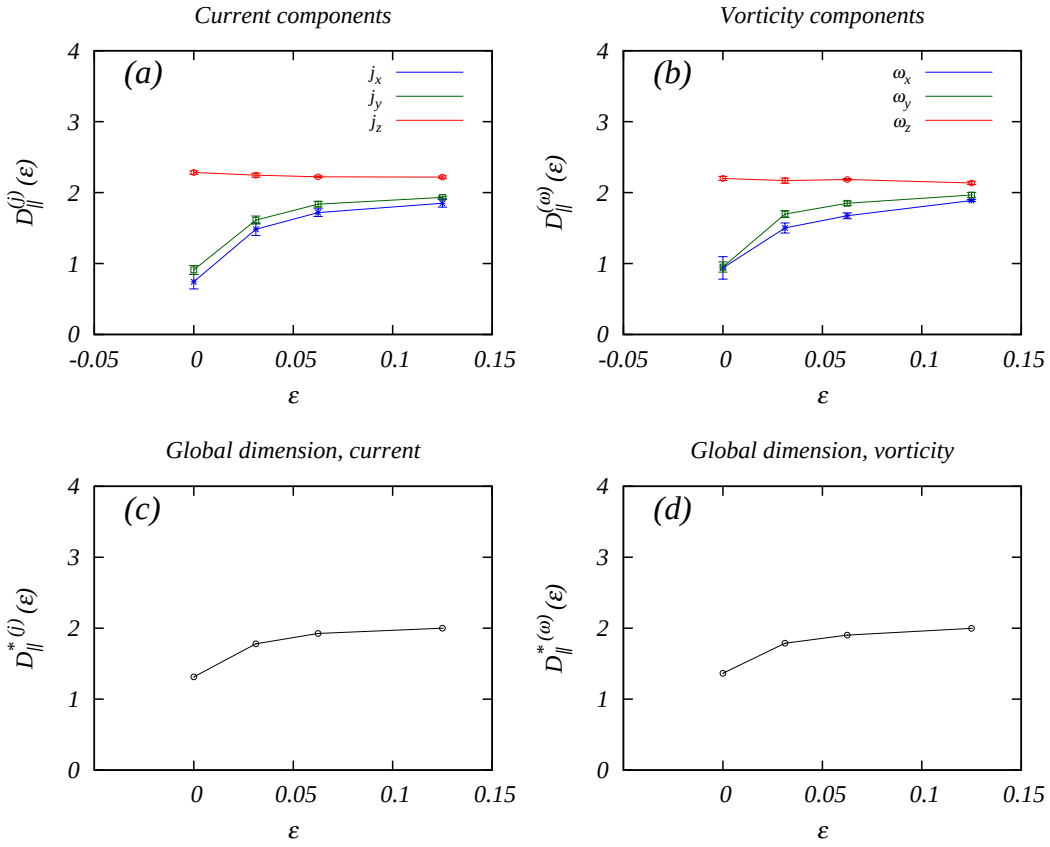

FIG. 10: The fractal dimension D of the parallel partition function, for the three components of current (left panels) and vorticity (right panels). The overall indicators $D_{\parallel}^{\star}$ are also plotted for the two fields (bottom panels).

as the presence of an active nonlinear turbulent cascade generating structures (i.e. parts of the fields with persistent sign) on all scales. The cancellation exponents, mesaured by fitting the partition functions, indicate the degree of cancellation occurring between structures of opposite sign, and are related to the gross fractal dimension of the typical turbulent structures in the flow. In the MHD range, current structures are only weakly sensitive to the Hall effect, showing slightly decreasing fractal dimension in particular in the perpendicular current components. The vorticity structures have a more evident fragmentation, suggesting that velocity and magnetic field may have decoupled dynamics in this range. In the Hall range, current and vorticity have similar behaviour, showing increasingly unraveled structures. The nonlinear Hall term is thus responsible for disruption and unraveling of the MHD current sheets, and for the generation of small scale structures.

The results obtained here, together with previous analysis [30, 41], provide a comprehensive approach that might answer the basic question: do the sheets get wider or narrower with the Hall effect? We can conclude that the Hall term has dual effects on the current sheets at different scales. On one hand, it increases the "macroscale" of the sheets by proportionally increasing their characteristic size. On the other hand, it causes these structures to unravel, which corresponds to generating microstructures on smaller scales. The decrease of the fractal dimension is a manifestation of the emerging microscales, while the widening of the macroscale of the sheet produces an increase of the filling factor of these microstructures, and the subsequent reduction of the observed intermittency [41].

These results may settle both the numerical and observational debate about the widening *vs* narrowing of the current sheets, which was probably due the extremely complex nature of the structures. Therefore, more comprehensive analysis, based on multiple approach to the same set of data (global magnitudes, characteristic times, energy cascade, intermittency, geometrical and topological properties) is desirable in order to fully understand the effect of the Hall term on the flow dynamics, and in particular on the topological characteristics of the current sheets. This work, along with Refs. [30, 41], may be an example of such comprehensive approach.

Acknowledgments

PD acknowledge support from the Carrera del Investigador Científico of CONICET. The authors acknowledge support from grants PICT 2011-1626 and 2011-1529, PIP 11220090100825, and UBACYT 20020110200359. We acknowledge support from the Marie Curie Project FP7 PIRSES-2010-269297 - "Turboplasmas".

[1] P. D. Mininni, D. O. Gómez, and S. M. Mahajan, Astrophys. **J. 584**, 1120 (2003).
[2] F. Mozer, S. Bale, and T. D. Phan, Phys. Rev. Lett. **89**, 015002 (2002).
[3] D. Smith, S. Ghosh, P. Dmitruk, and W. H. Matthaeus, Geophys. Res. Lett. **31**, 02805, DOI: 10.1029/2003GL018689 (2004).
[4] L. F. Morales, S. Dasso, and D. O. Gómez, J. Geophys. Res. **110**, A04204, DOI: 10.1029/2004JA010675 (2005).
[5] M. Wardle, Mon. Not. R. Astron. Soc. **303**, 239 (1999).
[6] S. A. Balbus and C. Terquem, Astrophys. **J. 552**, 235 (2001).
[7] W. H. Matthaeus, P. Dmitruk, D. Smith, S. Ghosh, and S. Ounghton, Geophys. Res. Lett. **30**, 2104, DOI: 10.29/2003GL017949 (2003).
[8] P. D. Mininni, D. O. Gómez, and S. M. Mahajan, Astrophys. **J. 619**, 1019 (2005).
[9] S. Galtier, J. Plasma Phys. **72**, 721 (2006).
[10] P. Dmitruk and W. H. Matthaeus, Phys. Plasmas **13**, 2307 (2006).
[11] D. O. Gomez, S. M. Mahajan, and P. Dmitruk, Phys. Plasma **15**, 102303 (2008).
[12] L. N. Martin, P. Dmitruk, Phys. Plasma **17**, 112304 (2010).
[13] N. H. Bian and D. Tsiklauri, Phys. Plasma **16**, 064503 (2009).
[14] G. P. Zank and W. H. Matthaeus, J. Plasma Phys. **48**, 85 (1992).
[15] A. A. van Ballegooijen, Astrophys. J. **311**, 1001 (1986).
[16] D. W. Longcope, and R. N. Sudan, Astrophys. J. **437**, 491 (1994).
[17] D. L. Hendrix and G. van Hoven, Astrophys. J. **467**, 887 (1996).
[18] L. Milano, P. Dmitruk, C. H. Mandrini, D. O. Gómez, and P. Demoulin, Astrophys. J. **521**, 889 (1999).
[19] D. O. Gómez, and C. Ferro Fontán, Astrophys. J. **394**, 662 (1992).
[20] P. Dmitruk and D. O. Gómez, Astrophys. J. Lett. **527**, L63 (1999).
[21] G. Nigro, F. Malara, V. Carbone, P. Veltri, Phys. Rev. Lett **92**, 194501 (2004).
[22] G. Nigro, F. Malara, P. Veltri, Astrophys. J. **685**, 606 (2008).
[23] P. Dmitruk, D. O. Gómez, and W. H. Matthaeus, Phys. Plasmas **10**, 3584 (2003).
[24] S. Oughton, P. Dmitruk, and W. H. Matthaeus, Phys. Plasmas **11**, 2214 (2004).
[25] P. Dmitruk, W. H. Matthaeus, and S. Oughton, Phys. Plasmas **12**, 112304 (2005).
[26] P. Dmitruk and W. H. Matthaeus, Phys. Plasmas **13**, 042307 (2006).
[27] J. Birn and M. Hesse, J. Geophys. Res. **106**, 3737 (2001).
[28] Y. Ren, M. Yamada, S. Gerhardt, H. Ji, R. Kulsrud, and A. Kuritsyn, Phys. Rev. Lett. **95**, 55003 (2005).
[29] M. Shay, J. F. Drake, B. N. Rogers, and R. E. Denton, J. Geophys. Res. **106**, 3759 (2001).
[30] L. N. Martin, P. Dmitruk, and D. O. Gómez, Phys. Plasmas, **19**, 052305 (2012).

[31] S. Donato, S. Servidio, P. Dmitruk, V. Carbone, M. A. Shay, and P. A. Cassak, Phys. Plasmas, **19**, 092307 (2012).

[32] P. D. Mininni, D. O. Gómez, and S. M. Mahajan, Astrophys. J. **567**, L81 (2002).

[33] P. D. Mininni, D. O. Gómez, and S. M. Mahajan, Astrophys. J. **584**, 1120 (2003).

[34] P. D. Mininni, D. O. Gómez, and S. M. Mahajan, Astrophys. J. **619**, 1019 (2005).

[35] P. D. Mininni, A. Alexakis and A. Pouquet, J. Plasma Phys. **73**, 377 (2007).

[36] D. O. Gómez, P. D. Mininni, and P. Dmitruk, Phys. Rev. E **82**, 036406 (2010).

[37] M. Yamada, Y. Ren, H. Ji, J. Breslau, S. Gerhardt, R. Kulsrud, and A. Kuritsyn, Phys. Plasmas, **13**, 052119 (2006).

[38] O. Alexandrova, V. Carbone, P. Veltri, and L. Sorriso-Valvo, Pl. and Space Sc. **55**, 2224 (2007).

[39] O. Alexandrova, V. Carbone, P. Veltri, and L. Sorriso-Valvo, Astrophys. J. **674**, 1153 (2008).

[40] K. H. Kiyani, S. C. Chapman, Yu. V. Khotyaintsev, and M. W. Dunlop and F. Sahraoui, Phys. Rev. Lett. **103**, 075006 (2010).

[41] P. Rodriguez Imazio, L. N. Martin, and P. D. Mininni, Phys. Plasma, "is tentatively scheduled for publication in the June, 2013

[42] M. Wan, S. Oughton, S. Servidio and W.H. Matthaeus, Phys. Plasmas **17**, 082308 (2010).

[43] E. Ott, Du. K. R. Sreenivasan, A. Juneja, and A. K. Suri, Phys. Rev. Lett. **69**, 2654 (1992).

[44] L. Sorriso-Valvo, V. Carbone, A. Noullez and H. Politano, A. Pouquet, P. Veltri, Phys. Plasmas, **9**, 89-95 (2002).

[45] D. Montgomery, Phys. Scripta, **T2**, 83 (1982).

[46] H. R. Strauss, Phys. Fluids, **19**, 134 (1976).

[47] D. O. Gómez, S. M. Mahajan, and P. Dmitruk, Phys. Plasmas, **15**, 102303 (2008).

[48] L. N. Martin, P. Dmitruk, and D. O. Gomez, Phys. Plasma **17**, 112304 (2010).

[49] S. Ghosh, M. Hossain, and W. H. Matthaeus, Phys. Commun. **74**, 18 (1993).

[50] U. Frisch, *Turbulence: The legacy of A.N. Kolmogorov*, Cambridge Univ. Press, Cambridge, UK (1995).

[51] A. Brandenburg, I. Procaccia and D. Segel, Phys. Plasmas **2**, 1148 (1995).

[52] H. Politano, A. Pouquet and P. L. Sulem, Phys. Plasmas **2** (8), 2931 (1995).

[53] R. M. Kerr and A. Brandenburg, Phys. Rev. Lett. **83** 1155 (1999).

[54] D. Biskamp and H. Welter, Phys. Fluids B **1**, 1964 (1989).

[55] H. Karimabadi et al., Phys. Plasmas **20**, 012303 (2013)

[56] P. Veltri, Plasma Phys. Cont. Fus. **41**, A787-A79 (1999).

[57] C. Salem, A. Mangeney, S.D. Bale, P. Veltri, Astrophys. J. **702**, 537-553 (2009).

[58] A. Greco, P. Chuychai, W. H. Matthaeus, S. Servidio, P. Dmitruk, Geophys. Res. Lett. **35**, L19111 (2008).

[59] D. Sundkvist, A. Retinò, A. Vaivads, S. D. Bale, Phis. Rev. Lett. **99**, 025004 (2007).

[60] S. I. Vainshtein, Y. Du, and K. R. Sreenivasan, Phys. Rev. E **49**, R2521 (2007).

[61] A. L. Bertozzi and A. B. Chhabra, Phys. Rev. E **49**, 4716 (1994).

[62] Graham, J., P. D. Mininni, and A. Pouquet, Phys. Rev. E **72**, 045301(R) (2005).

[63] V. B. Yurchyshyn, V. I. Abramenko, and V. Carbone, Astrophys. J., **538**, 968 (2000).

[64] V. I. Abramenko, V. B. Yurchyshyn, and V. Carbone, Solar Phys. **178**, 35, (1998).

[65] L. Sorriso-Valvo, V. Carbone, P. Veltri, V. I. Abramenko, A. Noullez, H. Politano, A. Pouquet, V. B. Yurchyshyn, Planet. Space Sci. **52**, 937 943 (2004).

[66] D. Laveder, T. Passot, and P. L. Sulem,, Phys. Plasmas, **9**, 293-304 (2002).